

Bandstop-to-Bandpass Microwave Photonic Filter Using a Phase-Shifted Fiber Bragg Grating

Xiuyou Han, *Member, IEEE*, and Jianping Yao, *Fellow, IEEE, Fellow, OSA*

Abstract—A bandstop-to-bandpass microwave photonic filter (MPF) using a phase-shifted fiber Bragg grating (PS-FBG) and a dual-drive Mach–Zehnder modulator (DD-MZM) is proposed and experimentally demonstrated. The PS-FBG has an ultranarrow notch in the reflection band. The DD-MZM is employed to generate a phase-modulated or a quasi-single-sideband (QSSB) optical signal by controlling the bias voltage. By applying the phase-modulated or QSSB signal to the PS-FBG to suppress one sideband, a bandpass or a bandstop MPF is implemented. The MPF can be continuously tuned from bandstop to bandpass or vice versa by controlling the bias voltage applied to the DD-MZM. The frequency tuning can be simply done by tuning the wavelength of the optical carrier. The proposed MPF is experimentally evaluated. Continuous tuning from a bandstop to bandpass filter with a bandstop rejection as high as 60 dB and frequency tuning with a frequency tunable range as large as 10 GHz are demonstrated.

Index Terms—Bandpass filter, bandstop filter, microwave photonic filter, phase-shifted fiber Bragg grating.

I. INTRODUCTION

MICROWAVE photonic filters (MPFs) with advantages such as broad bandwidth and large tunability have been extensively researched in the last few years [1]–[3]. Among the many filtering functions, bandstop and bandpass filtering are two major functions which are widely used for applications such as in communications systems and warfare systems [4], [5]. Usually, an MPF, once implemented, can only perform one function. For some applications, however, it is required that an MPF can be tuned from bandstop to bandpass or vice versa. Several approaches have been proposed to implement a bandstop-to-bandpass filter. For example, a bandstop-to-bandpass filter was realized by switching the operation of a Mach–Zehnder modulator (MZM) between its maximum transmission point and minimum transmission point [6]. A bandstop-to-bandpass filter could also be implemented using a 2×1 MZM and an active

fiber Bragg grating (FBG) pair [7]. Two wavelengths were used. One wavelength is tuned to be identical to the central wavelength of the FBGs, the active FBG pair serves as a Fabry–Pérot resonator, to generate multiple taps, and thus a multi-tap delay-line filter with a narrow passband is achieved. The other wavelength is tuned away from the central wavelengths of the FBGs and thus an all-pass filter is implemented. Due to a π phase shift between the phase responses of the multi-tap delay line filter and the all-pass filter, the combination of the frequency responses of the two filters corresponding to a notch filter. Of course, if the second wavelength is switched off, the filter is simply a bandpass filter [7]. A bandstop-to-bandpass filter could also be implemented using two optical tunable bandpass filters to perform phase-modulation to intensity-modulation (PM-IM) conversion with one filter in a recirculating loop to form an infinite impulse response (IIR) bandpass filter and the other outside the loop with no circulation to form an all-pass filter [8]. Depending on the phase difference between the IIR bandpass and the all-pass filters, a notch or bandpass filter can be implemented [8]. The major limitation of the MPFs in [6]–[8] is that the filters can only be switched from bandstop to bandpass or vice versa, but cannot be continuously tuned with a tunable notch depth or a passband gain. In addition, the MPFs in [6]–[8] are delay-line filters which exhibit periodic spectral response. Due to a relative long time delay difference between two adjacent taps, the free spectral range (FSR) is small, which may limit the filters for wide-band applications. To avoid having periodic spectral response, in [9] a bandstop-to-bandpass MPF implemented based on a phase modulator and a high-birefringence FBG-based Fabry–Pérot filter was demonstrated. Due to PM-IM conversion in the FBG-based Fabry–Pérot filter which was connected as a transmission or reflection filter, an MPF with a passband or a notch was realized. Again, the spectral response of the filter can only be switched by connecting the FBG-based Fabry–Pérot filter in transmission or reflection. In addition, the filter was not frequency tunable. To implement a frequency-tunable bandstop-to-bandpass MPF, in [10] a stimulated-Brillouin-scattering-(SBS) based optical filter and a dual-drive Mach–Zehnder modulator (DD-MZM) were used. By using the SBS loss and gain spectra to suppress and amplify, respectively, the two sidebands of a microwave-modulated signal generated at the output of the DD-MZM, a bandpass or bandstop filter was implemented. The frequency could be tuned by tuning the wavelength of the SBS pumping source. Since an SBS process was involved, the filter was very complicated which requires a high power pumping source and a long fiber. In addition, the MPF has two stopbands or passbands. In [10], to avoid having two stopbands or passbands, a photodetector (PD) with a relatively narrow bandwidth

Manuscript received April 21, 2015; revised August 8, 2015 and October 14, 2015; accepted October 14, 2015. Date of publication October 25, 2015; date of current version November 20, 2015. This work was supported by the Natural Sciences and Engineering Research Council of Canada. The work of X. Han was supported in part by the China Scholarship Council and the Natural Science Foundation of Liaoning Province under Grant 201402002.

X. Han is with the Microwave Photonics Research Laboratory, School of Electrical Engineering and Computer Science, University of Ottawa, Ottawa ON K1N 6N5, Canada, and also with the School of Physics and Optoelectronic Engineering, Dalian University of Technology, Dalian 116024, China.

J. Yao is with the Microwave Photonics Research Laboratory, School of Electrical Engineering and Computer Science, University of Ottawa, Ottawa ON K1N 6N5, Canada (e-mail: jpyao@eecs.uottawa.ca).

Color versions of one or more of the figures in this paper are available online at <http://ieeexplore.ieee.org>.

Digital Object Identifier 10.1109/JLT.2015.2492818

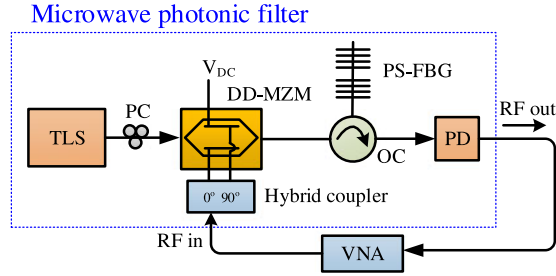


Fig. 1. The schematic of the proposed MPF. TLS, tunable laser source; DD-MZM, dual-drive Mach-Zehnder modulator; OC, optical circulator; PS-FBG, phase-shifted fiber Bragg grating; PD, photodetector; PC, polarization controller; VNA, vector network analyzer.

was used to eliminate the higher frequency band. Obviously, a PD with a narrow bandwidth will limit the frequency tunable range of the filter.

In this paper, we propose a simple approach to implementing a bandstop-to-bandpass MPF using a phase-shifted fiber Bragg grating (PS-FBG) and a DD-MZM, with only a single stopband or passband. The DD-MZM is employed to generate a phase-modulated or a quasi-single-sideband (QSSB) signal, realized by controlling the bias voltage to the DD-MZM. The PS-FBG has an ultra-narrow notch in the reflection band. By using the notch of the PS-FBG to suppress one sideband of the phase-modulated or the QSSB signal, a bandpass or bandstop filter is achieved. The MPF can be tuned from stopband to passband or vice versa by changing the bias voltage applied to the DD-MZM to change the power ratio between the two sidebands and the phase relationship. The frequency tuning can be simply done by tuning the frequency of the optical carrier. Compared with the approach in [10], the MPF has only a single stopband or passband, thus enabling a wider frequency tunable range. In addition, the use of a PS-FBG instead of an SBS-based filter makes the filter greatly simplified. The proposed MPF is experimentally evaluated. Continuous tuning of the MPF from bandstop to bandpass with a bandstop rejection as high as 60 dB and frequency tuning with a frequency tunable range as large as 10 GHz are demonstrated.

II. OPERATION PRINCIPLE

Fig. 1 shows the schematic of the proposed MPF. An optical carrier with a tunable frequency of f_c from a tunable laser source (TLS) is sent to a DD-MZM through a polarization controller (PC). The PC is adjusted to align the polarization direction of the optical carrier with the principal axis of the DD-MZM to minimize the polarization-dependent loss. The DD-MZM has dual microwave input ports connected to the two output ports of a 90° microwave hybrid coupler (HC). A microwave signal $V_e \cos(2\pi f_e t)$ with an amplitude voltage of V_e and a frequency of f_e is sent to the DD-MZM via the HC. The optical carrier is modulated by the input microwave signal at the DD-MZM. The microwave-modulated signal at the output of the DD-MZM is then sent and reflected by the PS-FBG via an optical circulator (OC), and detected at a PD. With the assumption of small signal

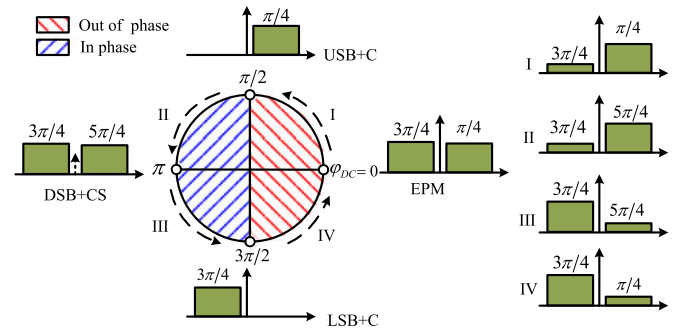


Fig. 2. The relationship between the static phase φ_{DC} controlled by the bias voltage to the DD-MZM and the combined magnitude of the two sidebands.

modulation, the electrical field of the optical signal at the output of the DD-MZM can be expressed as [11]:

$$E_{out1}(t) = E_{in} e^{j\frac{\varphi_{DC}}{2}} \times \left\{ \begin{array}{l} -J_{-1}(m) \cos\left(\frac{\varphi_{DC}}{2} + \frac{\pi}{4}\right) e^{j2\pi(fc-f_e)t} e^{j\frac{3\pi}{4}} \\ +J_0(m) \cos\left(\frac{\varphi_{DC}}{2}\right) e^{j2\pi fc t} \\ +J_1(m) \cos\left(\frac{\varphi_{DC}}{2} - \frac{\pi}{4}\right) e^{j2\pi(fc+f_e)t} e^{j\frac{\pi}{4}} \end{array} \right\} \quad (1)$$

where E_{in} is the amplitude of the optical carrier into the DD-MZM, the J_0 , J_{-1} , J_1 are the zero- and \pm first-order Bessel functions of the first kind; $m = \pi V_e / (2V_{\pi,e})$ is the modulation index; $\varphi_{DC} = \pi V_{DC} / V_{\pi,DC}$ is a static phase generated by the bias voltage V_{DC} ; $V_{\pi,e}$, and $V_{\pi,DC}$ are the half-wave voltages of the DD-MZM at the microwave and dc frequencies, respectively. From (1) we can see that the amplitude and phase of the two first-order sidebands can be controlled by φ_{DC} . Fig. 2 is a unit circle which shows the relationship between the static phase generated by the dc bias voltage and the combined magnitude of the two sidebands, given by $\sqrt{J_{-1}^2(m) + J_1^2(m)}$, which is a constant and is normalized to 1. By controlling the bias voltage, phase modulation or QSSB modulation can be achieved. For example, when φ_{DC} is adjusted to be 0, $\pi/2$, π and $3\pi/2$, four different modulations corresponding to equivalent phase modulation (EPM), upper sideband with carrier (USB+C) modulation, double sideband with suppressed carrier (DSB+CS) modulation, and lower sideband with carrier (SSB+C) modulation are, respectively, achieved. When φ_{DC} has a value other than the above four values, the amplitudes of the two sidebands are not equal, and the phase terms are $(3\pi/4, \pi/4)$ for $\varphi_{DC} \in (0, \pi/2)$ or $\varphi_{DC} \in (3\pi/2, 2\pi)$ in the first and fourth quadrants, and $(3\pi/4, 5\pi/4)$ for $\varphi_{DC} \in (\pi/2, \pi)$ or $\varphi_{DC} \in (\pi, 3\pi/2)$ in the second and the third quadrants.

The microwave-modulated signal at the output of the DD-MZM is fed to the PS-FBG via the OC. The PS-FBG is formed by introducing a phase shift, generally π , to a uniform FBG, to produce an ultra-narrow notch with the central frequency f_N in the reflection spectrum [12]. Here the PS-FBG is employed as a reflection filter and the electrical field of the reflected signal is

given by

$$E_{\text{out}2}(t) = E_{\text{in}} e^{j \frac{\varphi_{DC}}{2}} \times \left\{ \begin{array}{l} -\sqrt{r(f_C - f_e)} J_{-1}(m) \cos\left(\frac{\varphi_{DC}}{2} + \frac{\pi}{4}\right) \\ \cdot e^{[j2\pi(f_C - f_e)t + j\theta(f_C - f_e) + j\frac{3\pi}{4}]} \\ +\sqrt{r(f_C)} J_0(m) \cos\left(\frac{\varphi_{DC}}{2}\right) e^{[j2\pi f_C t + j\theta(f_C)]} \\ +\sqrt{r(f_C + f_e)} J_1(m) \cos\left(\frac{\varphi_{DC}}{2} - \frac{\pi}{4}\right) \\ \cdot e^{[j2\pi(f_C + f_e)t + j\theta(f_C + f_e) + j\frac{\pi}{4}]} \end{array} \right\} \quad (2)$$

where $r(f)$ and $\theta(f)$ are the normalized power spectrum and phase response of the PS-FBG given by [12]

$$r(f) = |H(f)|^2 \quad (3)$$

$$\theta(f) = \angle[H(f)] \quad (4)$$

where $H(f)$ is the transfer function of the PS-FBG given by [12]

$$H(f) = -\frac{{}^1F_{12}^2 F_{12} + {}^1F_{22}^2 F_{22} e^{j\varphi_{PS}}}{{}^1F_{11}^2 F_{21} + {}^1F_{21}^2 F_{21} e^{j\varphi_{PS}}} \quad (5)$$

$${}^iF_{11} = {}^iF_{22}^* = \cosh(\gamma L_i) - j \left(\frac{\hat{\sigma}}{\gamma} \right) \sinh(\gamma L_i) \quad (6)$$

$${}^iF_{12} = {}^iF_{21}^* = -j \left(\frac{\kappa}{\gamma} \right) \sinh(\gamma L_i) \quad (7)$$

where $i = 1, 2$ identifies two sub-gratings of the PS-FBG separated by the phase shift φ_{PS} , L_i is the corresponding sub-grating length, * denotes the complex conjugation, $\gamma^2 = \kappa^2 - \hat{\sigma}^2$, κ is the ‘‘ac’’ coupling coefficient defined as $\kappa = 2\pi f \Delta n / (2c)$ and Δn is the refractive index change, $\hat{\sigma}$ is the ‘‘dc’’ self-coupling coefficient defined as $\hat{\sigma} = n_{eff} 2\pi(f - f_D) / c$, n_{eff} is the effective refractive index, c is the velocity of light in vacuum, f is the frequency of the incident lightwave, and f_D is the frequency corresponding to the Bragg wavelength of the sub-FBGs.

The optical signal reflected from the PS-FBG is sent to the PD where the optical-to-electrical conversion is conducted. The recovered microwave signal is given by

$$i_e(t) \propto ac \{ \rho \cdot [E_{\text{out}2}(t) \cdot E_{\text{out}2}^*(t)] \} \approx A \left\{ \begin{array}{l} \sqrt{r(f_C - f_e)} \cos\left(\frac{\varphi_{DC}}{2} + \frac{\pi}{4}\right) \cdot \cos(2\pi f_e t + \theta_1) \\ +\sqrt{r(f_C + f_e)} \cos\left(\frac{\varphi_{DC}}{2} - \frac{\pi}{4}\right) \cdot \cos(2\pi f_e t + \theta_2) \end{array} \right\} \quad (8)$$

where

$$A = 2\rho |E_{\text{in}}|^2 \sqrt{r(f_C)} J_0(m) J_1(m) \cos(\varphi_{DC}/2) \quad (9)$$

$$\theta_1 = \theta(f_C) - \theta(f_C - f_e) - \frac{3\pi}{4} \quad (10)$$

$$\theta_2 = \theta(f_C + f_e) - \theta(f_C) + \frac{\pi}{4} \quad (11)$$

and $ac(\cdot)$ denotes the ac term of the output electrical signal, ρ is the responsivity of the PD. Note that the relationship of

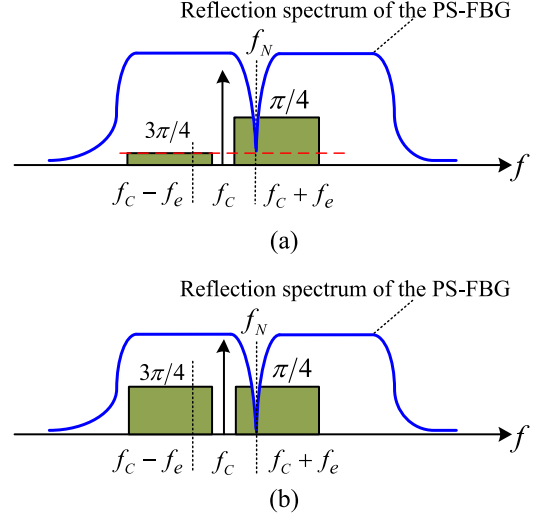


Fig. 3. The principle showing the operation of the MPF as (a) a bandstop or (b) a bandpass filter.

$J_{-1} = -J_1$ is used and only the fundamental frequency of the microwave signal is considered.

From (8) it can be seen that the microwave current at the output of the PD consists of two terms, and the amplitude and phase relationship between the two terms depends on the bias voltage applied to the DD-MZM. In fact, this relationship is resulted directly from the amplitude and phase relationship of the microwave-modulated signal, as shown in Fig. 3(a) and (b), in which the reflection spectrum of the PS-FBG is also shown. Assume the top of the magnitude spectrum of the PS-FBG is flat and the phase response in the reflection band is linear, the two sidebands of the microwave-modulated signal are within the reflection band and would have a phase relationship given by

$$\theta(f_C + f_e) - \theta(f_C) = \theta(f_C) - \theta(f_C - f_e) \quad (12)$$

$$\theta_2 - \theta_1 = \pi. \quad (13)$$

To implement a bandstop MPF, as shown in Fig. 3(a), φ_{DC} should have a value in quadrant I, as shown in Fig. 2, and the amplitude of the lower sideband is smaller than that of the upper sideband, which is called QSSB modulation. As can be seen from Fig. 3(a), if the notch of the PS-FBG is used to partially filter out the spectral component at $f_C + f_e$ in the upper sideband to make the amplitude identical to that of the lower sideband at $f_C - f_e$, a full cancellation of the two spectral components will be resulted due to the out of phase nature of the two sidebands [13], and a bandstop band filter with infinite notch depth is produced. The rejection ratio can be adjusted since the cancellation can be controlled by adjusting the bias voltage, which provides a better flexibility than the approach reported in [14], where no QSSB modulation was produced.

To implement a bandpass MPF, as shown in Fig. 3(b), φ_{DC} should be zero, and the DD-MZM is operating equivalently to a phase modulator with the modulated signal of two sidebands with identical amplitude, but a phase difference of π . If the PS-FBG is not used, the beating between the optical carrier and

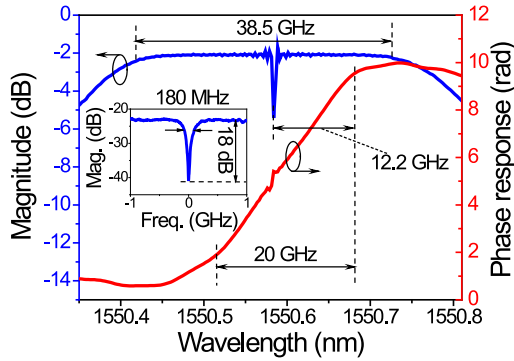


Fig. 4. The measured magnitude and phase responses of PS-FBG1. The inset provides a zoom-in view of the spectrum centered at the wavelength of the notch measured by the single sideband modulation technique.

one sideband will fully cancel the beating between the optical carrier and the other sideband. If the PS-FBG is used, however, the spectral component at the notch frequency, say, $f_C + f_e$, will not be cancelled, thus bandpass filter is produced.

The frequency tuning of the bandstop or bandpass filter can be done by simply tuning the wavelength of the optical carrier. Thus, a bandstop-to-bandpass MPF with both tunable notch depth and tunable frequency can be implemented.

III. EXPERIMENT

An experiment based on the configuration in Fig. 1 is performed. In the experiment, we use two PS-FBGs (PS-FBG1 and PS-FBG2) with different notch widths and different reflection bandwidths to demonstrate two MPFs with different stopband or passband widths and different tunable ranges. First, PS-FBG1 is used. An optical carrier from the TLS (YOKOGAMA AQ2200) is sent to the DD-MZM (Fujitsu, 10 GHz, $V_{\pi,e} = 5$ V) through the PC. The wavelength of the optical carrier is set at a wavelength greater than the central wavelength of the notch of PS-FBG1 and the upper sideband falls in the notch, as shown in Fig. 3. Fig. 4 gives the magnitude and phase responses of PS-FBG1 measured with an optical vector analyzer (LUNA, OVAe-4000). The wavelength of the notch is 1550.588 nm and the reflection band is about 39 GHz. The linear phase response region is about 20 GHz wide which is not perfectly symmetric relative to the notch wavelength. The microwave tunable range is about 6.1 GHz, a half of the right section 12.2 GHz of the linear phase response. The inset in Fig. 4. gives a zoom-in view of the spectrum centered at the notch wavelength measured by the single-sideband modulation technique [15], in which a frequency scanning microwave signal is modulated on an optical carrier to generate a single-sideband optical signal. By scanning the single sideband over the spectral range of the notch, the spectrum of the PS-FBG centered at the notch is measured with an ultra-high resolution [15]. The notch bandwidth is about 180 MHz and the rejection ratio is 18 dB.

A microwave signal from the VNA (Agilent E8364A) is applied to the DD-MZM via the HC (ARRA 9428X), with the two output ports of the HC connected to the two RF input ports of the DD-MZM. Note that a Bias-Tee is used to combine a dc

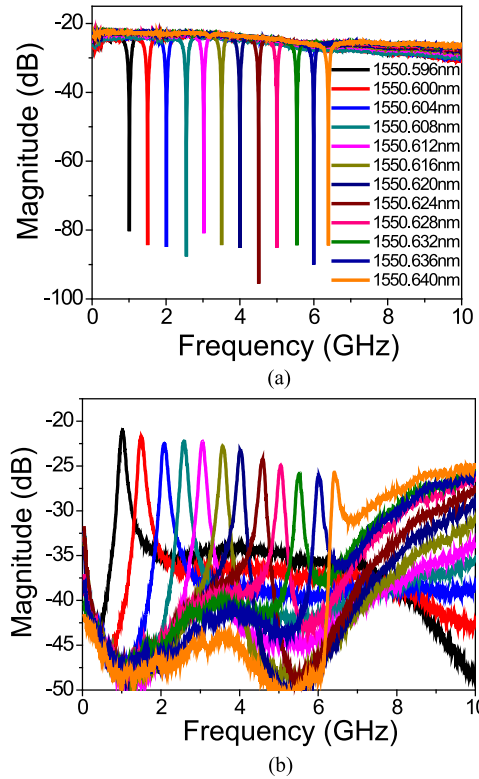


Fig. 5. The measured frequency response of the MPF when PS-FBG1 is employed. The spectral response when the MPF is operating as a (a) bandstop filter and (b) bandpass filter.

voltage with one of the microwave signals to provide the bias voltage. The power of the microwave signal to each of the two input ports of the DD-MZM is 6 dBm. The modulation index is calculated to be about 0.20, thus the small signal modulation is guaranteed. The microwave-modulated signal is sent to PS-FBG1 and reflected to the PD (New Focus, 25 GHz) via the OC. The recovered microwave signal is amplified by a microwave amplifier with a gain of 10 dB and is sent back to the VNA to measure the spectral response. The bias voltage from a dc power supply (KIKUSUI, 0.001 V) is tuned to control the amplitude and phase of the two sidebands.

The MPF operating as a bandstop filter is first demonstrated. The bias voltage is tuned such that the amplitude of the two sidebands meets the relationship as shown in Fig. 3(a). The frequency of the microwave signal from the VNA is swept from 0 to 10 GHz to measure the frequency response of the MPF, and the wavelength of the optical carrier from the TLS is tuned from 1550.596 to 1550.640 nm with a tuning step of 0.004 nm (or equivalently 0.5 GHz) to evaluate the frequency tunability. The frequency response is shown in Fig. 5(a), in which a deep notch with an ultra-high rejection ratio (> 55 dB) is shown over the entire frequency tuning range. The rejection ratio is much higher than that of PS-FBG1 (18 dB). This is because the tuning of the power ratio between the two sidebands by tuning the bias voltage enables a full cancellation of the two beat signals at the output of the PD.

Then, the MPF operating as a bandpass filter is demonstrated. By setting φ_{DC} to zero, the EPM is achieved, in which the two

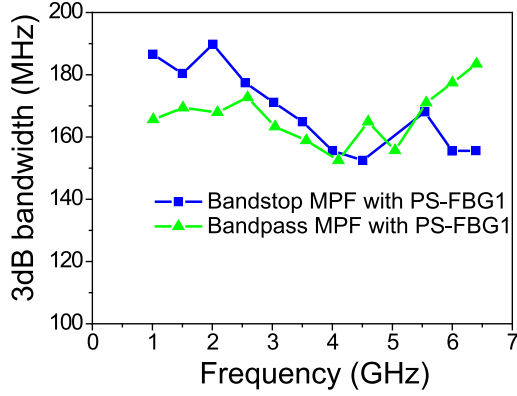


Fig. 6. The 3-dB widths of the stopband and passband of the MPF when using PS-FBG1.

sidebands have an identical amplitude and a π phase difference. By applying the modulated signal to PS-FBG1, as shown in Fig. 3(b), the upper sideband is eliminated by the notch of PS-FBG1, and the phase-modulated signal is converted to a single-sideband intensity-modulated signal. The entire operation corresponds to a bandpass filter. Again, the frequency tunability is achieved by tuning the wavelength of the optical carrier. The frequency response of the MPF is shown in Fig. 5(b).

Note that during the tuning process, due to the nonlinear phase response of PS-FBG1 near the two edges of the reflection band, the phase relationship between the two sidebands may not be always maintained, which may lead to a poor rejection ratio when operating as a bandstop MPF, and a lower passband gain when operating as a bandpass MPF. Therefore, to maintain a uniform rejection ratio or passband gain, the tunable range is controlled within the linear region of the phase response of PS-FBG1. For PS-FBG1, the frequency range corresponding to a linear phase response is about 20 GHz and is not symmetric relative to the notch wavelength. In the experiment, a section of about 12.2 GHz is used, which leads to a frequency tunable range of about 6.1 GHz.

The bandwidths of the notch and passband when the MPF is operating as a bandstop and a bandpass filter are measured. Fig. 6 shows the bandwidths when the MPF is tuned. Since PS-FBG1 has a notch with a width of 180 MHz, the widths of the notch and passband are around 180 MHz, with some variations due to the non-perfect cancellation of the two sidebands due to the non-ideal linear phase response of PS-FBG1.

The rejection ratio of the MPF operating as a bandstop filter can also be tunable, which is done by tuning the bias voltage to the DD-MZM to change the power ratio between the two sidebands. If the two sidebands are not fully cancelled, the rejection ratio would be reduced. Fig. 7 shows the measured frequency response of the MPF operating as a stopband filter with a tunable rejection ratio. In the experiment, the bias voltage is tuned at a step of 0.1 V. The inset in Fig. 7 shows the relationship between the rejection ratio and the bias voltage change relative to the bias voltage to achieve the highest rejection ratio.

Finally, the tuning of the MPF from bandstop to bandpass is demonstrated, which is done again by tuning the bias voltage. Fig. 8. shows the measured frequency response, where the MPF

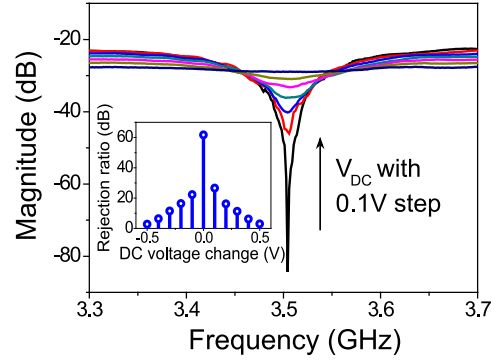


Fig. 7. The tuning of the rejection ratio when the MPF is operating as a bandstop filter. The inset shows the relationship between the rejection ratio of the bandstop filter and the bias voltage change relative to the bias voltage to achieve the maximum rejection ratio.

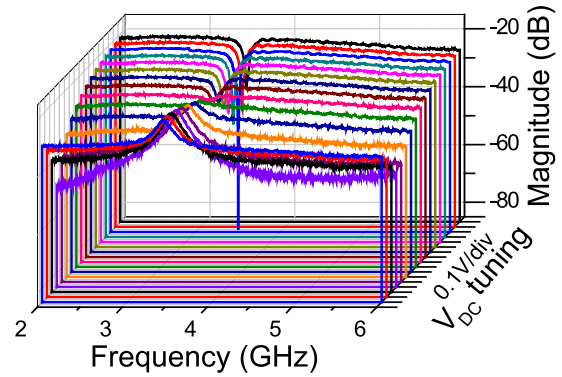


Fig. 8. The frequency response of the MPF when the filter is tuned from a bandstop filter to a bandpass filter.

is tuned to operate from a bandstop filter with a maximum rejection ratio of 60 dB and a bandpass filter with a maximum ratio of the transmission peak to the sidelobe of 20 dB.

The bandwidth and the frequency tunable range of the MPF are determined by the notch width and the reflection bandwidth of the PS-FBG used. In a second experiment, we use a second PS-FBG (PS-FBG2) with a narrower notch width and wider reflection bandwidth to replace PS-FBG1 to demonstrate an MPF with narrower notch width and wider frequency tunable range. Fig. 9 shows the magnitude and phase responses of PS-FBG2. The notch width is 10 MHz with a rejection ratio of 20 dB, and the reflection bandwidth is 70 GHz, in which 40 GHz can be used. Thus, the microwave frequency tunable range can be as large as 20 GHz.

We first demonstrate the operation of the MPF as a bandstop filter. To do so, the wavelength of the optical carrier from the TLS is set at a wavelength smaller than the central wavelength of the notch (1549.691 nm) of PS-FBG2, to take advantage of a wider spectral range to enable greater frequency tunable range. Fig. 10(a) shows the frequency response of the MPF as a bandstop filter with the optical wavelength tuned from 1549.680 to 1549.610 nm with a tuning step of -0.01 nm. Again, a high rejection ratio (> 40 dB) over a frequency tunable range of 10 GHz is obtained. The frequency tunable range is limited by the frequency response of the DD-MZM used in the experiment.

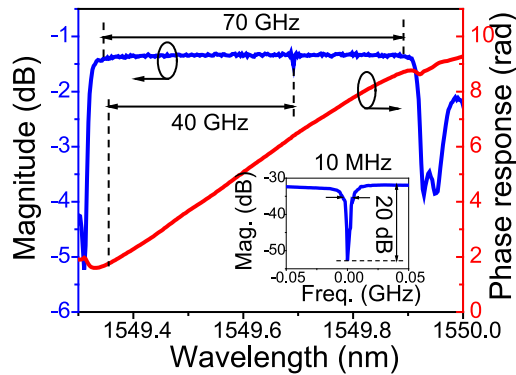


Fig. 9. The measured magnitude and phase responses of PS-FBG2. The inset provides a zoom-in view of the spectrum centered at the wavelength of the notch measured by the single-sideband modulation technique.

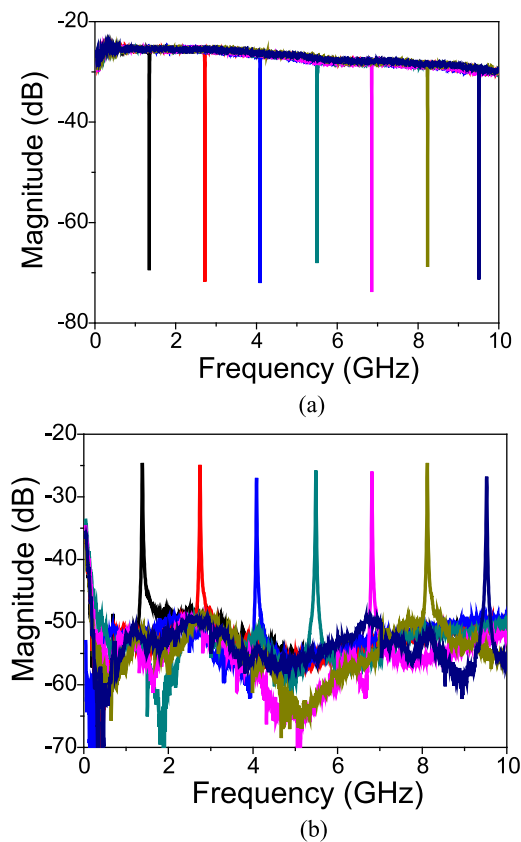


Fig. 10. The measured frequency response of the MPF when using PS-FBG2. The spectral response when the MPF is operating as a (a) bandstop filter and (b) bandpass filter.

If a DD-MZM with a wider bandwidth is used, the frequency of the MPF with PS-FBG2 can be tuned up to 20 GHz.

Then, we demonstrate the operation of the MPF as a bandpass filter. Again, the bias voltage is tuned such that the two sidebands have an identical amplitude and a π phase difference. The frequency tuning is done by tuning the wavelength of the TLS. Fig. 10(b) shows the frequency response of the MPF as a bandpass filter with a frequency tunable range of 10 GHz.

Since PS-FBG2 has a much narrower notch width, the MPF will have a much narrower notch or passband width. Fig. 11

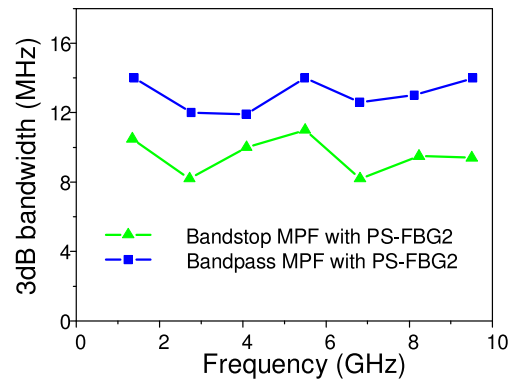


Fig. 11. The 3-dB widths of the stopband and passband of the MPF when using PS-FBG2.

shows the notch and passband widths of the MPF. As can be seen the notch widths are around 10 MHz when the filter is tuned over the 10 GHz range. The variations in the widths are due to again the non-ideal linear phase response of PS-FBG2, which leads to partial cancellation of the two beat signals at the output of the PD.

We should note that the rejection ratio of the bandstop filter using PS-FBG2 is poorer than the one with PS-FBG1. There are two factors that lead to the poorer rejection ratio. One is that the notch width of PS-FBG2 is much narrower than that of PS-FBG1, which makes the bandstop filter with PS-FBG2 is more sensitive to the fluctuations of the sideband amplitude of the QSSB optical signal. The other is that the bias voltage from the dc power supply is tuned manually, which is not precise and stable enough to ensure an accurate control. If a dc power supply with a higher precision and programmable control is utilized, an extremely high rejection ratio can be obtained for PS-FBG2 as well as PS-FBG1.

IV. DISCUSSION AND CONCLUSION

The frequency tunable range of the proposed filter was around 6 GHz (for PS-FBG1) and 10 GHz (for PS-FBG2). If the proposed filter is implemented using a PS-FBG with a wider reflection bandwidth, say, a chirped PS-FBG with a reflection bandwidth of 100 GHz or greater, the tunable range will be much greater, limited only by the bandwidths of the DD-MZM and the PD.

In conclusion, a bandstop-to-bandpass MPF using a PS-FBG and a DD-MZM was proposed and experimentally demonstrated. The fundamental concept of the approach was the use of a DD-MZM to achieve EPM or QSSB modulation by controlling the bias voltage. By using a PS-FBG to fully or partially suppress one sideband, an MPF with a stopband or a passband was implemented. The proposed MPF was experimentally demonstrated in which two different PS-FBGs, PS-FBG1 and PS-FBG2, with different notch widths and reflection bandwidths were employed. For PS-FBG1, an MPF with a notch width of 180 MHz and a frequency tunable range of 6 GHz was demonstrated. For PS-FBG2, an MPF with a notch width of 10 MHz and a frequency tunable range of 10 GHz was demonstrated. In

addition, continuous tuning of the MPF from a bandstop to a bandpass filter was also achieved.

REFERENCES

- [1] J. Capmany and D. Novak, "Microwave photonics combines two worlds," *Nature Photon.*, vol. 1, no. 6, pp. 319–330, Jun. 2007.
 - [2] J. Yao, "Microwave photonics," *J. Lightw. Technol.*, vol. 27, no. 3, pp. 314–335, Feb. 2009.
 - [3] R. A. Minasian, "Photonic signal processing of microwave signals," *IEEE Trans. Microw. Theory Technol.*, vol. 54, no. 2, pp. 832–846, Feb. 2006.
 - [4] J. Capmany, J. Mora, I. Gasulla, J. Sancho, J. Lloret, and S. Sales, "Microwave photonic signal processing," *J. Lightw. Technol.*, vol. 31, no. 43, pp. 571–586, Feb. 2013.
 - [5] R. A. Minasian, E. H. W. Chan, and X. Yi, "Microwave photonic signal processing," *Opt. Exp.*, vol. 21, no. 19, pp. 22918–22936, Sep. 2013.
 - [6] J. Capmany, J. Cascon, D. Pastor, and B. Ortega, "Reconfigurable fiber-optic delay line filters incorporating electrooptic and electroabsorption modulators," *IEEE Photon. Technol. Lett.*, vol. 11, no. 9, pp. 1174–1176, Sep. 1999.
 - [7] E. H. W. Chan, "All-optical reconfigurable microwave photonic signal processor," *Microw. Opt. Technol. Lett.*, vol. 50, no. 8, pp. 1989–1991, Aug. 2008.
 - [8] Y. Yu, E. Xu, J. Dong, L. Zhou, X. Li, and X. Zhang, "Switchable microwave photonic filter between high Q bandpass filter and notch filter with flat passband based on phase modulation," *Opt. Exp.*, vol. 18, no. 24, pp. 25271–25282, Nov. 2010.
 - [9] R. Tao, X. Feng, Y. Cao, Z. Li, and B. Guan, "Tunable microwave photonic notch filter and bandpass filter based on high-birefringence fiber-Bragg-grating-based Fabry–Pérot cavity," *IEEE Photon. Technol. Lett.*, vol. 24, no. 20, pp. 1805–1808, Oct. 2012.
 - [10] W. Zhang and R.A. Minasian, "Switchable and tunable microwave photonic Brillouin-based filter," *IEEE Photon J.*, vol. 4, no. 5, pp. 1443–1455, Oct. 2012.
 - [11] B. Hraimel, M.O. Twati, and K. Wu, "Closed-form dynamic range expression of dual-electrode Mach–Zehnder modulator in radio-over-fiber WDM system," *J. Lightw. Technol.*, vol. 24, no. 6, pp. 2380–2387, Jun. 2006.
 - [12] T. Erdogan, "Fiber grating spectra," *J. Lightw. Technol.*, vol. 15, no. 8, pp. 1277–1294, Aug. 1997.
 - [13] D. Marpaung, B. Morrison, R. Pant, C. Roeloffzen, A. Leinse, M. Hoekman, R. Heideman, and B. J. Eggleton, "Si₃N₄ ring resonator-based microwave photonic notch filter with an ultrahigh peak rejection," *Opt. Exp.*, vol. 21, no. 20, pp. 23286–23294, Oct. 2013.
 - [14] J. Dong, L. Liu, D. Gao, Y. Yu, A. Zheng, T. Yang, and X. Zhang, "Compact notch microwave photonic filters using on-chip integrated microring resonators," *IEEE Photon. J.*, vol. 5, no. 2, p. 5500307, Apr. 2013.
 - [15] Z. Tang, S. Pan, and J. P. Yao, "A high resolution optical vector network analyzer based on a wideband and wavelength-tunable optical single sideband modulator," *Opt. Exp.*, vol. 20, no. 6, pp. 6555–6560, Mar. 2012.
- Xiuyou Han** (M'13) received the Ph.D. degree in optical engineering from the Shanghai Institute of Optics and Fine Mechanics, Chinese Academy of Sciences, Shanghai, China, in 2006.
- In 2006, he joined the School of Physics and Optoelectronic Engineering, Dalian University of Technology, Dalian, China, as a Lecturer, where he became an Associate Professor in 2009. He is currently a Visiting Scholar in the Microwave Photonics Research Laboratory, School of Electrical Engineering and Computer Science, University of Ottawa, ON, Canada. His current research interests include microwave photonics and integrated photonics.
- Jianping Yao** (M'99–SM'01–F'12) received the Ph.D. degree in electrical engineering from the Université de Toulon, Toulon, France, in December 1997. He is a Professor and the University Research Chair in the School of Electrical Engineering and Computer Science, University of Ottawa, Ottawa, ON, Canada. He joined the School of Electrical and Electronic Engineering, Nanyang Technological University, Singapore, as an Assistant Professor in 1998. In December 2001, he joined the School of Electrical Engineering and Computer Science, University of Ottawa, as an Assistant Professor, where he became an Associate Professor in 2003, and a Full Professor in 2006. He was appointed University Research Chair in Microwave Photonics in 2007. From July 2007 to June 2010, he was the Director of the Ottawa-Carleton Institute for Electrical and Computer Engineering. He was re-appointed as the Director of the Ottawa-Carleton Institute for Electrical and Computer Engineering in 2013.
- Dr. Yao has published more than 490 papers, including more than 290 papers in peer-reviewed journals and 200 papers in conference proceedings. He was a Guest Editor for the Focus Issue on Microwave Photonics in *Optics Express* in 2013 and a Feature Issue on Microwave Photonics in *Photonics Research* in 2014. He is currently a Topical Editor for Optics Letters, and serves on the Editorial Board of the IEEE Transactions on Microwave Theory and Techniques, Optics Communications, and China Science Bulletin. He is a Chair of numerous international conferences, symposia, and workshops, including the Vice Technical Program Committee (TPC) Chair of the IEEE Microwave Photonics Conference in 2007, the TPC Co-Chair of the Asia-Pacific Microwave Photonics Conference in 2009 and 2010, the TPC Chair of the high-speed and broadband wireless technologies subcommittee of the IEEE Radio Wireless Symposium in 2009–2012, the TPC Chair of the microwave photonics subcommittee of the IEEE Photonics Society Annual Meeting in 2009, the TPC Chair of the IEEE Microwave Photonics Conference in 2010, the General Co-Chair of the IEEE Microwave Photonics Conference in 2011, the TPC Co-Chair of the IEEE Microwave Photonics Conference in 2014, and the General Co-Chair of the IEEE Microwave Photonics Conference in 2015. He received the 2005 International Creative Research Award at the University of Ottawa. He received the 2007 George S. Glinski Award for Excellence in Research. He was selected to receive an inaugural OSA Outstanding Reviewer Award in 2012. He is an IEEE MTT-S distinguished microwave Lecturer for 2013–2015. He is a registered Professional Engineer of Ontario. He is a Fellow of the Optical Society of America and the Canadian Academy of Engineering.